Article

Identification of an Early–Middle Jurassic oxidized magmatic belt, south Gangdese, Tibet, and geological implications

Yinqiao Zou [a,b], Xilian Chen [a,b], Wenting Huang [a], Jian Zhang [a,b], Huaying Liang [a,*], Jifeng Xu [c], Ling Chen [d]

[a] Key Laboratory of Mineralogy and Metallogeny, Guangzhou Institute of Geochemistry, Chinese Academy of Sciences, Guangzhou 510640, China
[b] University of Chinese Academy of Sciences, Beijing 100049, China
[c] State Key Laboratory of Isotope Geochemistry, Guangzhou Institute of Geochemistry, Chinese Academy of Sciences, Guangzhou 510640, China
[d] Guangxi Key Laboratory of Marine Disaster in the Beibu Gulf, Qinzhou University, Qinzhou 535011, China

A B S T R A C T

The south Gangdese region is the site of subduction of the Neo-Tethys and subsequent continental collision. Compared with widespread Cretaceous and Cenozoic magmatism, Early–Middle Jurassic magmatic rocks and related deposits are rarely reported. Our work identified a >200 km long felsic rock belt associated with Cu mineralization in the south Gangdese region. We report here zircon U–Pb ages, zircon Ce^{4+}/Ce^{3+} values, and mineral assemblages of two Cu mineralized intrusions within the belt. A hornblende granite and a diorite porphyry were emplaced at 177.3 Ma and 166.3 Ma, respectively. Geological occurrence and magmatic hematite–magnetite–chalcopyrite intergrowths suggest that Cu mineralization formed coeval with Jurassic intrusions. Mineralized intrusions have high zircon Ce^{4+}/Ce^{3+} and Eu_N/Eu_N^* ratios, and hematite–magnetite intergrowths, suggesting their parent magmas were highly oxidized. Hornblende is common and primary fluid inclusions are found in titanite and apatite, indicating their parent magmas were water-saturated and exsolved volatile phases at early stage of magmatic evolution. Those magma characters contribute to the formation of porphyry Cu deposits. Given that majority subduction-related porphyry Cu systems have been eroded following uplift and denudation, the well-preserved Early–Middle Jurassic Cu mineralized igneous rocks in south Gangdese are favorable prospecting targets for subduction-related porphyry Cu deposits.

© 2017 Science China Press. Published by Elsevier B.V. and Science China Press. All rights reserved.

1. Introduction

The south Gangdese region was the site of Mesozoic subduction of Neo-Tethys oceanic crust and subsequent Cenozoic collision of the Indian with Eurasian plates [1]. Numerous collision-related porphyry Cu(Mo) deposits have been identified in the south Gangdese belt [2–9]. The collision-related porphyries associated with Cu(Mo) mineralization have isotope data ranging mainly from 13 to 18 Ma [2–8]. Petrogenesis of the porphyries has been a subject of debate. The main opinions on petrogenesis of the collision-related porphyries include that the magmas were derived from subducted oceanic crust [10], from subducted Indian mafic lower crust mixing with the Lhasa lower crust components [11], from thickened juvenile mafic crust [2], from subduction-modified lower crust with contribution from lithosphere mantle [12], and from an upper mantle source metasomatised by slab-derived melts [13]. However, the subduction related porphyry deposits are rare

found in comparison with the collision related porphyry deposits, only the Xiongcun super-large porphyry Cu(Au) deposit was related to the northward subduction of the Neo-Tethys oceanic crust during the Middle Jurassic [14,15]. Tang et al. [15] argued that the Xiongcun porphyry Cu(Au) deposit was formed in an intra-oceanic island arc setting [15] and Kang et al. [16], on the other hand, proposed that the Jurassic igneous rocks in the south Gangdese were form at the continental margin [16]. Given that porphyry deposits occurred mainly in the supra-subduction zone in arc setting [17], why subduction-related porphyry Cu(Au) deposits are rare in the south Gangdese region? Thus, further work is required, focusing on the temporal–spatial distribution and geochemical features of subduction-related felsic igneous rocks in the south Gangdese. Such work would help determine if subduction-related felsic igneous rocks contributed to the formation of porphyry Cu(Au) deposits.

We describe here a series of mineralized volcanic rocks and intrusions in the south Gangdese region, and analyze zircon LA–ICP–MS U–Pb isotopes and geochemical features of the Cu-mineralized intrusions. This work is critical to analyses of the

temporal–spatial distribution of the subduction-related igneous rocks and to assessing the potential for subduction-related porphyry Cu(Au) deposits in the south Gangdese.

2. Geological background

The Gangdese belt is a giant magmatic belt located between the Yarlung Zangbo and Bangong–Nujiang suture zones, extending ~2500 km from west to east and 150–300 km from north to south [18] (Fig. 1). The belt records the opening and closure of the Neo-Tethys Ocean, and collision of the Indian and Eurasian plates [1]. Magmatic rocks related to continental collision are widespread in the south Gangdese. Previous geological, geophysical, and geochemical studies indicate that plate collision started at 50–65 Ma [19–21].

Cenozoic granites [22,23] and minor Cretaceous arc granites [24–27] are widely exposed in the south Gangdese, due to large-scale uplift and denudation caused by collision between the Indian and Eurasian plates since ~65 Ma. Multiple collision-related porphyry Cu–Mo deposits of Miocene age (18–13 Ma) occur in the Gangdese belt, forming an important porphyry Cu–Mo deposit belt in the south Gangdese [2–8]. Previous studies have shown that the south Gangdese belt was subducted along with Neo-Tethyan oceanic crust prior to the Jurassic [16]. However, Early–Middle Jurassic subduction-related porphyry Cu(Au) deposits are not widespread

in the south Gangdese. Recently, the Xiongcun porphyry Cu–Au deposit was identified in the south Gangdese [15,28,29], and the mineralization is thought to have been triggered by subduction of Neo-Tethys oceanic crust [14,30].

3. Geological features

We conducted systematic field investigations in the south Gangdese region, from Xietongmen in the west to Quxu in the east, revealing that associations of volcanic rocks and intrusions are widely distributed in a zone of >200 km in length (west to east) (Fig. 1b). The volcanic rocks and intrusions are characterized by Cu mineralization and quartz–epidote veins and alteration, whereas the surrounding Cenozoic intrusions are unaltered.

One such intrusion is located 10 km east of Xietongmen County, Xigaze (Fig. 1b and c). The intrusion is covered by diluvium and volcanic sedimentary rocks, and is only exposed in several deep valleys (Fig. 2a). A pink Cretaceous biotite–K-feldspar granite crops out to the west of the intrusion. Based on field observations, the intrusion is estimated to be >5 km^2 in surface area (Fig. 1c). The intrusion underwent Cu mineralization (Fig. 2b) and quartz–epidote vein alteration (Fig. 2c), whereas the adjacent Cretaceous biotite–K-feldspar granite to the west is unaltered. The mineralized intrusion is medium- to coarse-grained, with typical granitic textures, and it has a mineral assemblage of plagioclase (45%–55%),
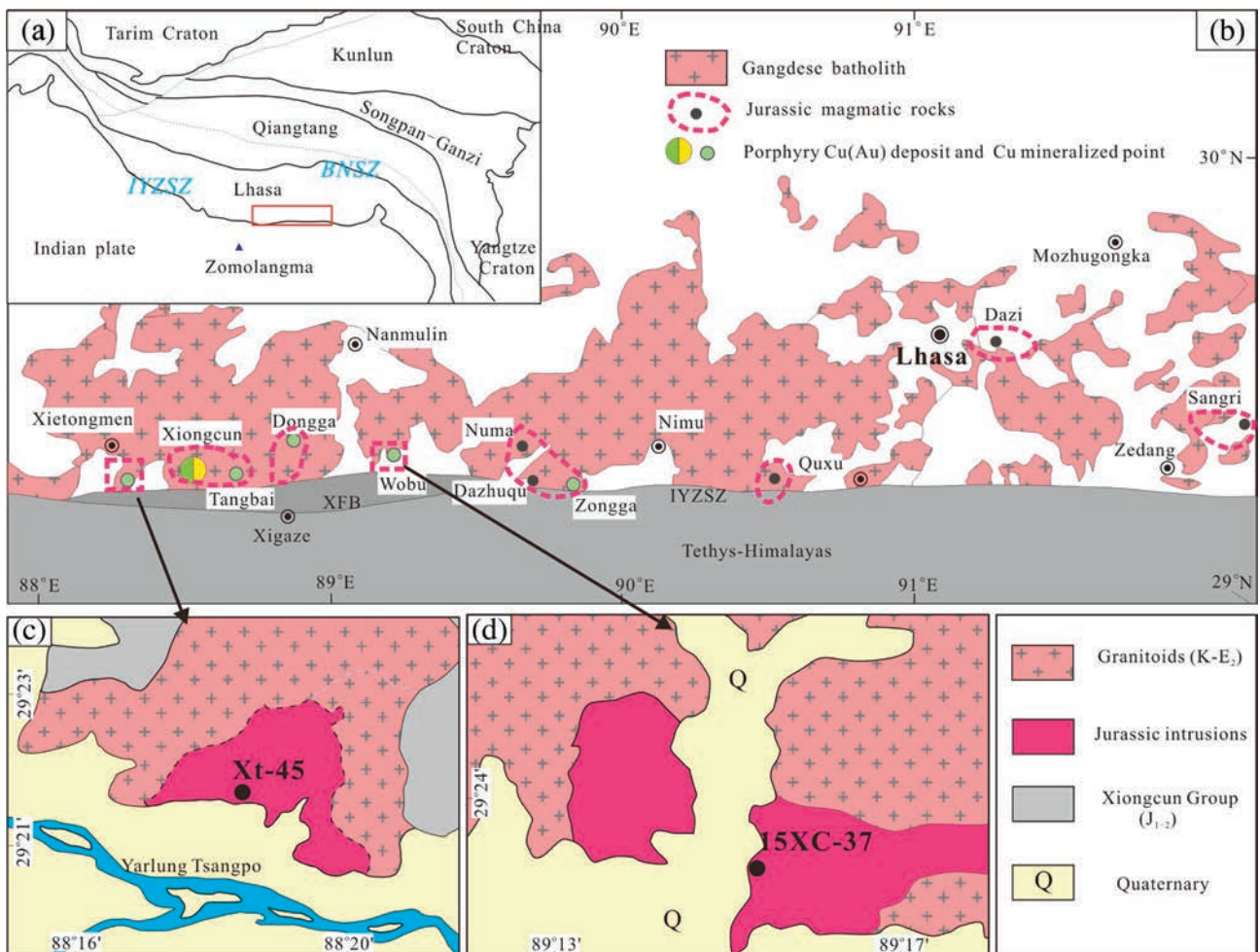
Fig. 1. Sketch region geological map of the south Gangdes belt. (a) Tectonic sketch of the Tibet Plateau; (b) The distribution of magmatic rocks in the south Gangdese, modified after [15]; Mineralized Jurassic igneous rocks are located by this study and some Jurassic intrusions are based on [26,48–50,52,55]; (c) Simple geological maps of hornblende granite and (d) diorite porphyry. Abbreviation: BNSZ – Bangong Nujiang suture zone; IYZSZ – Indus Yarlung Zangbo suture zone; XFB – Xigaze forearc basin.
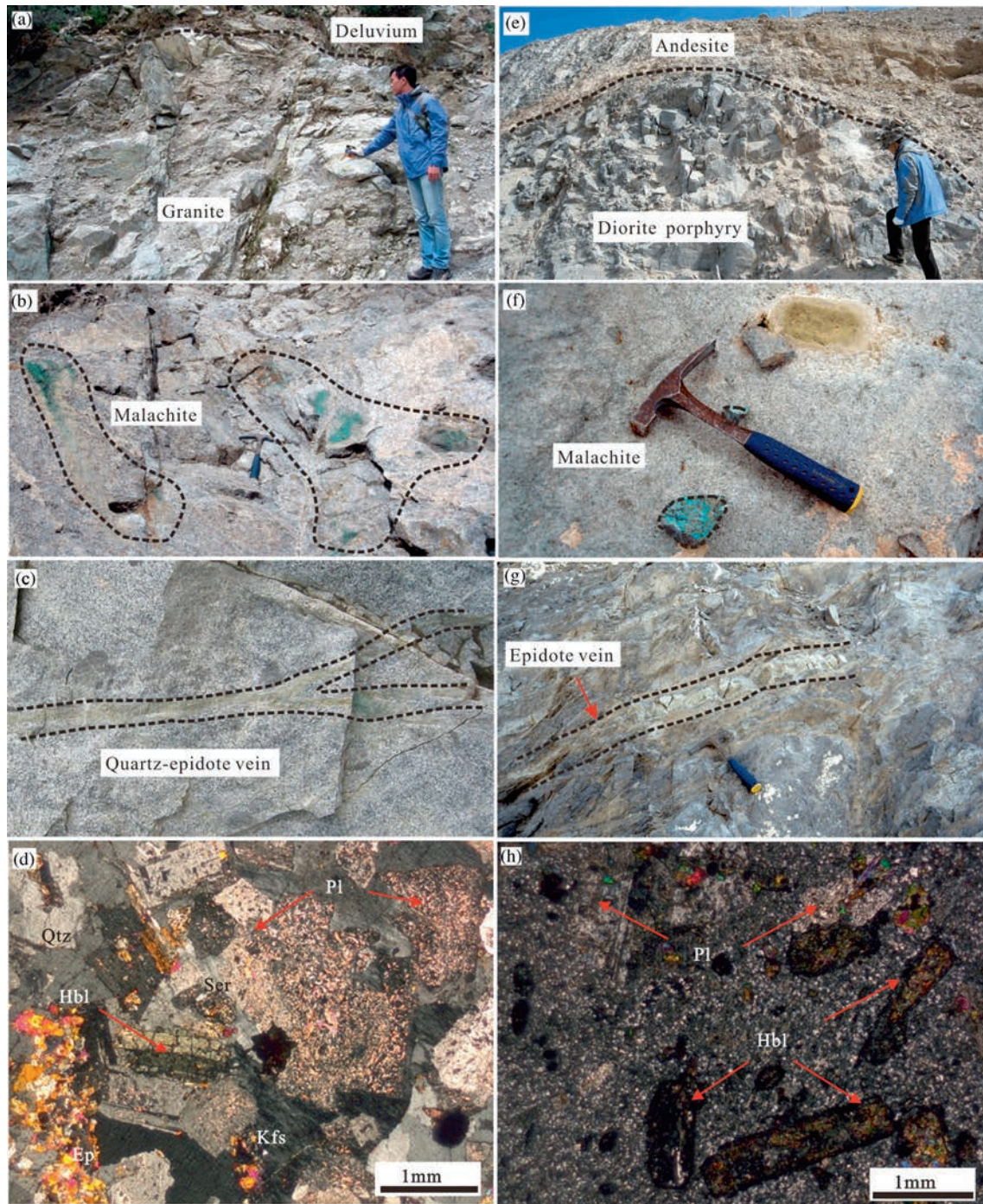
Fig. 2. Photographs showing the characteristics of hornblende granite and diorite porphyry. (a) Deluvium and granite, (b) Cu mineralization in hornblende granite, (c) quartz–epidote vein alteration in hornblende granite, (d) texture and mineral assemblage of hornblende granite, (e) diorite porphyry and associated andesite, (f) malachite mineralization in diorite porphyry, (g) epidote vein alteration in andesite, (h) texture and mineral assemblage of the diorite porphyry. Abbreviation: Qtz – quartz; Hbl – hornblende; Pl – plagioclase; Ser – sericite; Ep – epidote; Kfs – K – feldspar.

quartz (20%–30%), hornblende (3%–8%), and K-feldspar (5%–10%), as well as minor magnetite and accessory titanite, apatite, and zircon (Fig. 2d). There is evidence of sericitization and epidote–chlorite alteration of plagioclase and hornblende crystals. The mineral assemblages and textures indicate that the intrusion is a hornblende granite.

A second mineralized intrusion occurs near Aima County, Xigaze (Fig. 1b–d). This intrusion is associated with andesite (Fig. 2e), volcanic breccia, and overlying tuff, and is exposed in a quarry and several valleys. The surface area of the intrusion is

estimated to be <10 km². The intrusion underwent Cu mineralization (Fig. 2f) and epidote–chlorite alteration (Fig. 2g), whereas the surrounding Cenozoic biotite granites are unaltered. The second intrusion has a porphyritic texture, with phenocrysts of plagioclase (15%–20%) and hornblende (18%–25%) in a matrix of quartz, plagioclase, minor K-feldspar, and accessory apatite and magnetite (Fig. 2e). Phenocrysts of plagioclase and hornblende show evidence of sericitization, carbonation, and epidote–chlorite alteration. The textures and mineral assemblage of these rocks indicate that the intrusion is a diorite porphyry.
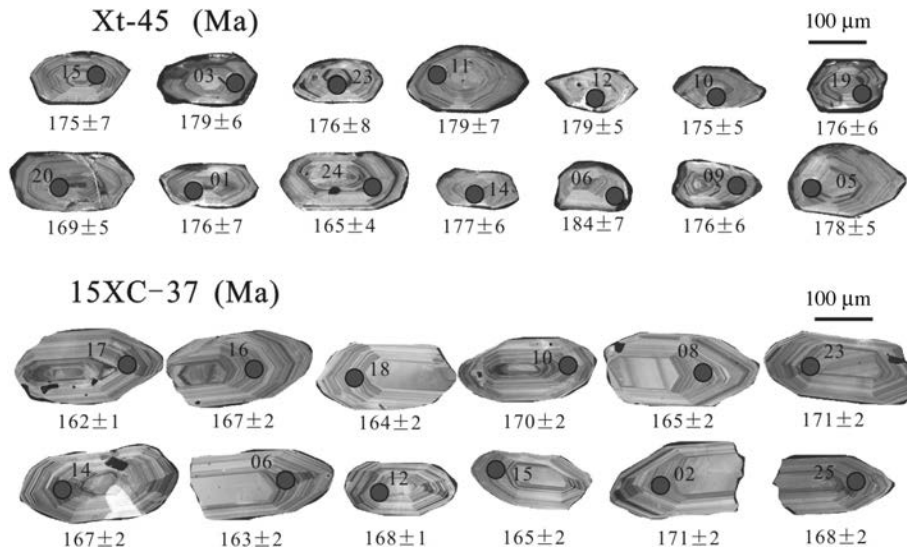
Table 1
Zircon U–Pb isotope data, Ce^{4+}/Ce^{3+} and Eu_N/Eu_N^* values of analyzed intrusions.

Analyzed No.	Th ppm	U ppm	Th/U	Ce^{4+}/Ce^{3+}	Eu_N/Eu_N^*	$^{207}Pb/^{206}Pb$	±1s.e.	$^{207}Pb/^{235}U$	±1s.e.	$^{206}Pb/^{238}U$	±1s.e.	$^{207}Pb/^{235}U$ Ages	±1s.e.	$^{206}Pb/^{238}U$ Ages	±1s.e.	Concordance
Hornblende granite																
Xt45-01	47	100	0.47	1040	0.39	0.04913	0.01306	0.19035	0.04930	0.02769	0.00124	176.9	42.1	176.1	7.8	99%
Xt45-02	86	156	0.55	584	0.36	0.05770	0.01231	0.21601	0.04044	0.02991	0.00111	198.6	33.8	190.0	7.0	95%
Xt45-03	72	130	0.55	334	0.44	0.05061	0.00751	0.19541	0.02792	0.02822	0.00096	181.2	23.7	179.4	6.0	98%
Xt45-04	64	130	0.49	342	0.46	0.06145	0.01163	0.20996	0.03719	0.02612	0.00101	193.5	31.2	166.2	6.4	84%
Xt45-05	169	267	0.63	1155	0.43	0.05446	0.00864	0.20072	0.03002	0.02814	0.00095	185.7	25.4	178.9	5.9	96%
Xt45-06	149	206	0.72	1253	0.43	0.04333	0.00802	0.18699	0.03938	0.02909	0.00112	174.1	33.7	184.9	7.0	93%
Xt45-07	110	191	0.57	666	0.42	0.04826	0.00722	0.19995	0.03048	0.02825	0.00084	185.1	25.8	179.6	5.2	96%
Xt45-08	78	171	0.45	870	0.44	0.05301	0.00803	0.17839	0.02537	0.02604	0.00097	166.7	21.9	165.7	6.1	99%
Xt45-09	86	161	0.54	578	0.41	0.04827	0.00748	0.19053	0.02817	0.02775	0.00097	177.1	24.0	176.5	6.1	99%
Xt45-10	111	160	0.69	723	0.6	0.04968	0.00756	0.18977	0.02907	0.02763	0.00091	176.4	24.8	175.7	5.7	99%
Xt45-11	68	129	0.52	308	0.72	0.05346	0.01228	0.20140	0.04157	0.02817	0.00122	186.3	35.1	179.1	7.6	96%
Xt45-12	84	173	0.49	843	0.42	0.04866	0.00694	0.19786	0.02670	0.02827	0.00084	183.3	22.6	179.7	5.3	98%
Xt45-13	72	134	0.54	1720	0.42	0.04782	0.01194	0.18328	0.04271	0.02818	0.00111	170.9	36.7	179.1	7.0	95%
Xt45-14	127	187	0.68	1055	0.46	0.04934	0.00970	0.18894	0.03530	0.02786	0.00099	175.7	30.2	177.1	6.2	99%
Xt45-15	59	113	0.52	157	0.5	0.03955	0.01226	0.18458	0.05600	0.02760	0.00117	172.0	48.0	175.5	7.3	97%
Xt45-16	108	181	0.60	16463	0.6	0.05123	0.00778	0.20814	0.03087	0.02886	0.00088	192.0	26.0	183.4	5.5	95%
Xt45-17	138	236	0.58	911	0.36	0.05214	0.00751	0.21209	0.02871	0.03092	0.00147	195.3	24.1	196.3	9.2	99%
Xt45-18	89	141	0.63	318	0.44	0.05438	0.01221	0.19011	0.04243	0.02742	0.00113	176.7	36.2	174.4	7.1	98%
Xt45-19	72	139	0.52	162	0.53	0.04650	0.00908	0.18671	0.03619	0.02778	0.00099	173.8	31.0	176.6	6.2	98%
Xt45-20	318	342	0.93	373	0.35	0.04836	0.00562	0.17583	0.02013	0.02661	0.00086	164.5	17.4	169.3	5.4	97%
Xt45-21	139	253	0.55	808	0.42	0.04956	0.00658	0.19672	0.02424	0.03013	0.00112	182.3	20.6	191.3	7.0	95%
Xt45-22	44	110	0.40	579	0.5	0.05505	0.00864	0.19609	0.02856	0.02939	0.00154	181.8	24.3	186.7	9.6	97%
Xt45-23	77	152	0.51	491	0.58	0.05421	0.00873	0.18820	0.03436	0.02776	0.00128	175.1	29.4	176.5	8.0	99%
Xt45-24	118	220	0.54	403	0.49	0.05214	0.00686	0.18994	0.02532	0.02598	0.00075	176.6	21.6	165.3	4.7	93%
Xt45-25	48	98	0.49	2224	0.67	0.06644	0.02880	0.17605	0.06299	0.02564	0.00124	164.7	54.4	163.2	7.8	99%
Diorite porphyry																
15XC-37-01	454	720	0.63	349	0.43	0.04844	0.00141	0.18142	0.00550	0.02722	0.00033	169.3	4.7	173.1	2.0	97%
15XC-37-02	300	529	0.57	327	0.44	0.05031	0.00179	0.18519	0.00672	0.02681	0.00031	172.5	5.8	170.6	1.9	98%
15XC-37-03	622	813	0.77	283	0.37	0.05110	0.00147	0.18663	0.00531	0.02664	0.00031	173.8	4.5	169.5	1.9	97%
15XC-37-04	725	849	0.85	298	0.42	0.05122	0.00153	0.17996	0.00525	0.02553	0.00019	168.0	4.5	162.5	1.2	96%
15XC-37-05	505	628	0.80	390	0.4	0.05019	0.00180	0.18222	0.00702	0.02624	0.00029	170.0	6.0	167.0	1.8	98%
15XC-37-06	443	635	0.70	297	0.44	0.04766	0.00159	0.16707	0.00531	0.02563	0.00031	156.9	4.6	163.2	2.0	96%
15XC-37-07	432	601	0.72	353	0.42	0.04977	0.00177	0.18317	0.00636	0.02676	0.00027	170.8	5.5	170.3	1.7	99%
15XC-37-08	678	802	0.85	294	0.4	0.04828	0.00133	0.17172	0.00459	0.02597	0.00030	160.9	4.0	165.3	1.9	97%
15XC-37-09	626	816	0.77	283	0.39	0.05241	0.00148	0.18097	0.00486	0.02513	0.00022	168.9	4.2	160.0	1.4	94%
15XC-37-10	308	573	0.54	352	0.4	0.04889	0.00151	0.17841	0.00539	0.02667	0.00031	166.7	4.6	169.7	2.0	98%
15XC-37-11	1218	1439	0.85	328	0.36	0.04935	0.00102	0.16703	0.00357	0.02453	0.00020	156.8	3.1	156.2	1.3	99%
15XC-37-12	613	801	0.77	304	0.44	0.05014	0.00171	0.18139	0.00597	0.02639	0.00023	169.3	5.1	167.9	1.5	99%
15XC-37-13	494	849	0.58	333	0.36	0.05120	0.00157	0.18075	0.00534	0.02569	0.00024	168.7	4.6	163.5	1.5	96%
15XC-37-14	779	1002	0.78	321	0.4	0.05093	0.00118	0.18342	0.00423	0.02621	0.00026	171.0	3.6	166.8	1.6	97%
15XC-37-15	762	915	0.83	263	0.4	0.05120	0.00121	0.18278	0.00452	0.02593	0.00027	170.5	3.9	165.0	1.7	96%
15XC-37-16	495	770	0.64	348	0.41	0.04885	0.00144	0.17656	0.00521	0.02624	0.00025	165.1	4.5	167.0	1.6	98%
15XC-37-17	704	892	0.79	300	0.37	0.04945	0.00127	0.17341	0.00452	0.02546	0.00029	162.4	3.9	162.1	1.8	99%
15XC-37-18	634	820	0.77	348	0.39	0.05447	0.00226	0.19244	0.00735	0.02576	0.00025	178.7	6.3	163.9	1.6	91%
15XC-37-19	644	855	0.75	251	0.42	0.05280	0.00163	0.18789	0.00558	0.02600	0.00026	174.8	4.8	165.4	1.7	94%
15XC-37-20	807	902	0.89	97	0.44	0.07265	0.00228	0.25975	0.00938	0.02562	0.00029	234.5	7.6	163.1	1.8	64%
15XC-37-21	576	773	0.74	324	0.4	0.05018	0.00156	0.17877	0.00556	0.02594	0.00026	167.0	4.8	165.1	1.7	98%
15XC-37-22	615	807	0.76	244	0.44	0.05265	0.00165	0.19286	0.00597	0.02681	0.00032	179.1	5.1	170.6	2.0	95%
15XC-37-23	381	594	0.64	299	0.43	0.05170	0.00172	0.19089	0.00644	0.02683	0.00033	177.4	5.5	170.7	2.1	96%
15XC-37-24	499	727	0.69	275	0.42	0.05046	0.00178	0.17876	0.00627	0.02588	0.00033	167.0	5.4	164.7	2.1	98%
15XC-37-25	683	801	0.85	118	0.45	0.05460	0.00155	0.19817	0.00569	0.02639	0.00024	183.6	4.8	167.9	1.5	91%

Xt-45 (Ma)

175±7   179±6   176±8   179±7   179±5   175±5   176±6

169±5   176±7   165±4   177±6   184±7   176±6   178±5

15XC-37 (Ma)

162±1   167±2   164±2   170±2   165±2   171±2

167±2   163±2   168±1   165±2   171±2   168±2

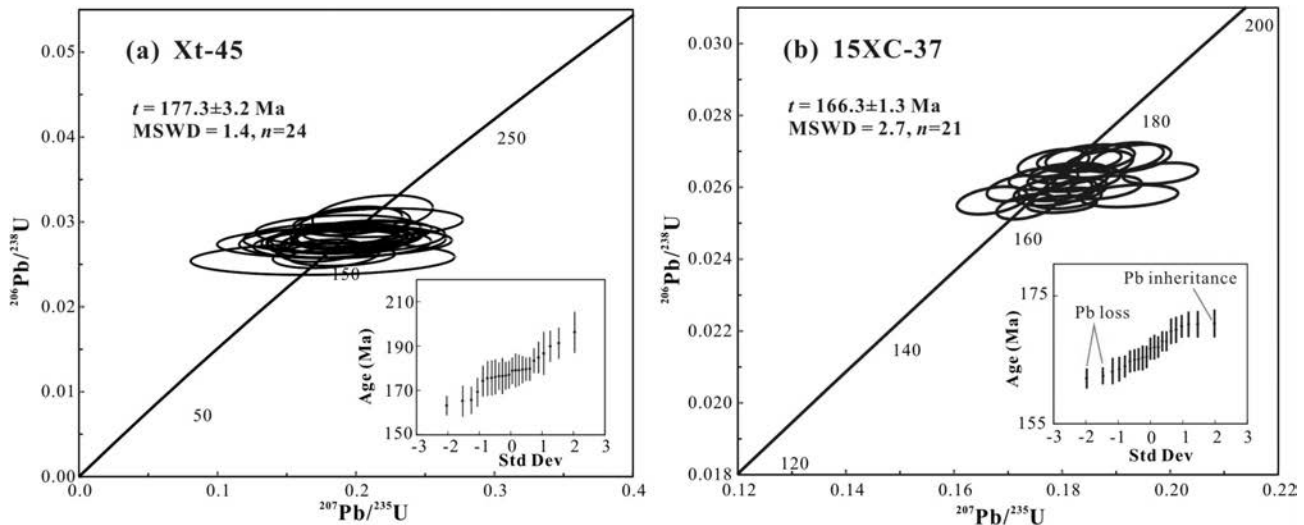**Fig. 3.** CL images of representative zircon grains of samples of Xt-45 and 15XC-37.

Fig. 4. Zircon U-Pb concordia diagrams of the two mineralized intrusions. The inserts are probability plots. (a) Hornblende granite, (b) diorite porphyry.

4. Samples and analytical methods

Samples of the hornblende granite (Xt-45; 88°18′02″E, 29°21′35″N) and diorite porphyry (15XC-37; 89°14′45″E 29°24′N) were collected for analysis of zircon U–Pb isotopes. Zircon grains were separated using conventional heavy liquid and magnetic separation techniques. Separated zircon grains were hand-picked, then mounted in epoxy resin and polished to approximately half their thickness. Cathodoluminescence (CL) images were taken to reveal their external and internal structures. A laser ablation–inductively coupled plasma–mass spectrometer (LA–ICP–MS) was used for zircon U–Pb isotopic analyses at the State Key Laboratory of Continental Dynamics, Department of Geology, Northwest University, China. Detailed procedures and instrumental parameters are described by [31]. Soft ICPMSDataCal 7.2 and Isoplot were used for data processing and calculations [32,33].

Twenty-five zircon grains were analyzed per sample and data with concordance <90% were discarded. The remaining data were processed using cumulative probability plots to determine if the data belong to the main population. The zircon grains from a single age population typically have calculated mean standard weighted deviation (MSWD) values of <3 [34]. If the MSWDs values are significantly >3, old and young U–Pb outliers were interpreted to be inherited zircons and zircons suffered Pb loss, respectively. The U–Pb ages determined in this way are interpreted as representing the crystallization age of the intrusion [34,35]. Zircon Ce^{4+}/Ce^{3+} and Eu_N/Eu_N^* values were calculated using the same method of data analysis, and details of the theory that underlies the calculation are reported by [36].

5. Results

LA–ICP–MS zircon U–Pb isotopic data are listed in Table 1, and CL images and concordia plots for the analyzed zircon grains are shown in Figs. 3 and 4, respectively. All of the analyzed zircons display oscillatory zoning (Fig. 3) and show high Th/U ratios (0.47–0.93), indicating a magmatic origin.

The hornblende granite (sample Xt-45) yields a weighted mean zircon U–Pb age of 177.3 ± 3.2 Ma, with MSWD = 1.4 (Fig. 4a). The two zircon grains suffered Pb loss and one inherited zircon grain

are discarded (the insert probability plot in Fig. 4b). The diorite porphyry (sample 15XC-37) yields a weighted mean zircon U–Pb age of 166.3 ± 1.3 Ma, with MSWD = 2.7 (Fig. 4b).

The zircon Ce^{4+}/Ce^{3+} and Eu_N/Eu_N^* ratios were determined for all zircon grains (Table 1). The hornblende granite (Xt-45) yields zircon Ce^{4+}/Ce^{3+} ratios of 157–16,463 (average 1374) and Eu_N/Eu_N^* ratios of 0.35–0.72 (average 0.47). The diorite porphyry (15XC-37) yields zircons Ce^{4+}/Ce^{3+} ratios of 97–389 (average 295) and Eu_N/Eu_N^* ratios of 0.36–0.45 (average 0.41) (Table 1).

6. Discussion

6.1. Chronology

The zircon crystals analyzed in this study display oscillatory zoning and high Th/U ratios (0.47–0.93), indicating a magmatic origin. The main population of zircon ages is interpreted to represent the crystallization age of the intrusion. The hornblende granite and diorite porphyry were emplaced at 177.3 Ma and 166.3 Ma, respectively (Fig. 4). The two intrusions underwent Cu mineralization and have similar zircon U–Pb ages to the Xiongcun porphyry Cu–Au deposit in the south Gangdese belt [14]. These features suggest that the rocks are all genetically related to subduction of the Neo-Tethys slab [14,15].

6.2. Geochemical features of magmas favoring porphyry Cu(Au) mineralization

6.2.1. High oxidization

Most porphyry Cu deposits are generated from highly oxidized magmas [37–40]. Many previous studies have attempted to determine the oxygen fugacity of porphyries associated with Cu(Au) mineralization, revealing that magmatic zircon Ce^{4+}/Ce^{3+} and Eu_N/Eu_N^* values, and iron oxide mineral assemblages in the rocks might record the oxygen fugacity of the parent melts [34,36,41–43].

The hornblende granite and diorite porphyry have relatively high zircon Ce^{4+}/Ce^{3+} and Eu_N/Eu_N^* values (Table 1). In a Ce^{4+}/Ce^{3+} vs. Eu_N/Eu_N^* diagram, the two mineralized intrusions are consistent with the data from the Xiongcun porphyry Cu(Au) deposit that all fall in the same area as Chuquicamata–El Abra ore-bearing samples in Chile [36] (Fig. 5). The zircon grains from the hornblende granite and diorite porphyry have high Ce^{4+}/Ce^{3+} and Eu_N/Eu_N^* values, indicating their parent magmas were highly oxidized. The hornblende granite has a mineral assemblage that includes titanite, magnetite, and quartz (Fig. 6a). This assemblage is interpreted to have crystallized from a highly oxidized melt [44–46]. The highly oxidized signatures of the hornblende granite and diorite porphyry are further supported by the fact that both rocks contain iron-oxide assemblage of the form of magnetite–hematite intergrowths (Fig. 6b–d), which is commonly observed in many large porphyry deposits [42].

6.2.2. High water content

Hornblende crystallization is strongly influenced by the water content of magma. Abundant hornblendes will crystallize earlier if the water content of a melt is >4% [38]. The hornblende granite and diorite porphyry of the present study contain high concentrations of hornblende (Fig. 2d and h), indicating the parent magmas were water-rich. Water-saturated magma can exsolve volatile phases during the early stages of magmatic evolution, and fluid inclusions may form when contemporaneous magmatic minerals crystallize from the water-saturated melt [3,47]. Accessory minerals such as titanite and apatite crystallize at the early stage of crystalline sequence and can provide important records for magma signature. Many fluid inclusions occur in titanite and apatite of hornblende granite and apatite of diorite porphyry (Fig. 7). The fluid inclusions with diameter of 1–10 μm appear randomly in the accessory mineral with rounded isometric (Fig. 7a-1, b-1) or
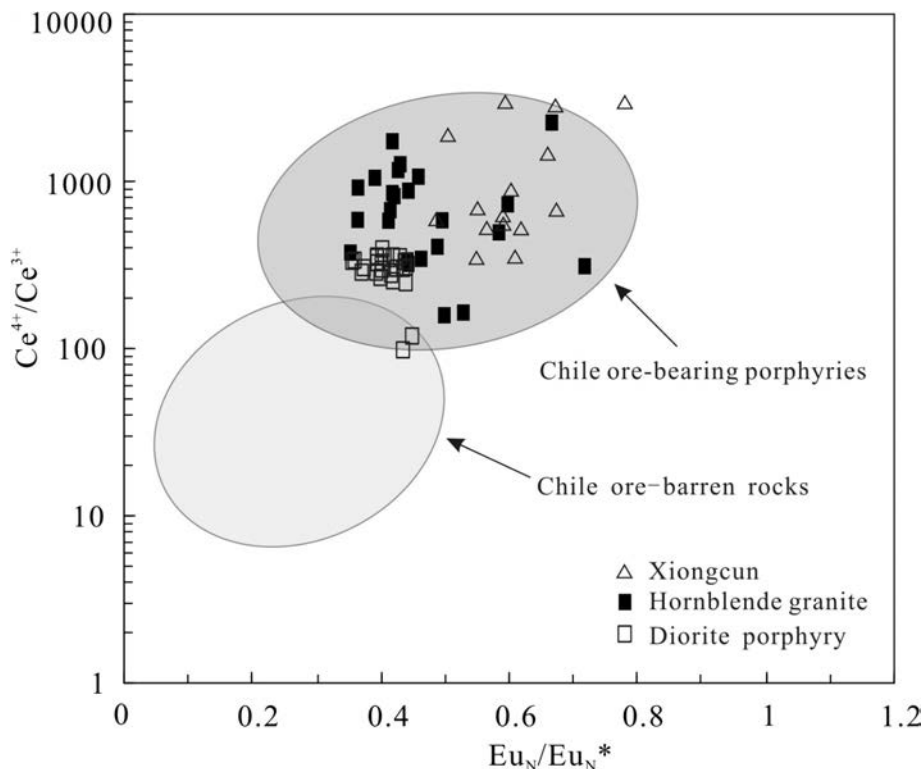
Fig. 5. Plot of Zircon Ce^{4+}/Ce^{3+} vs Eu_N/Eu_N^*. The Cu mineralization hornblende granite and diorite porphyry are located at the same domain as the Chuquicamata–El Abra giant porphyry Cu deposit in Chile. Data of Chile ore-barren and ore-bearing porphyry were from [36]; data of Xiongcun were from [29].
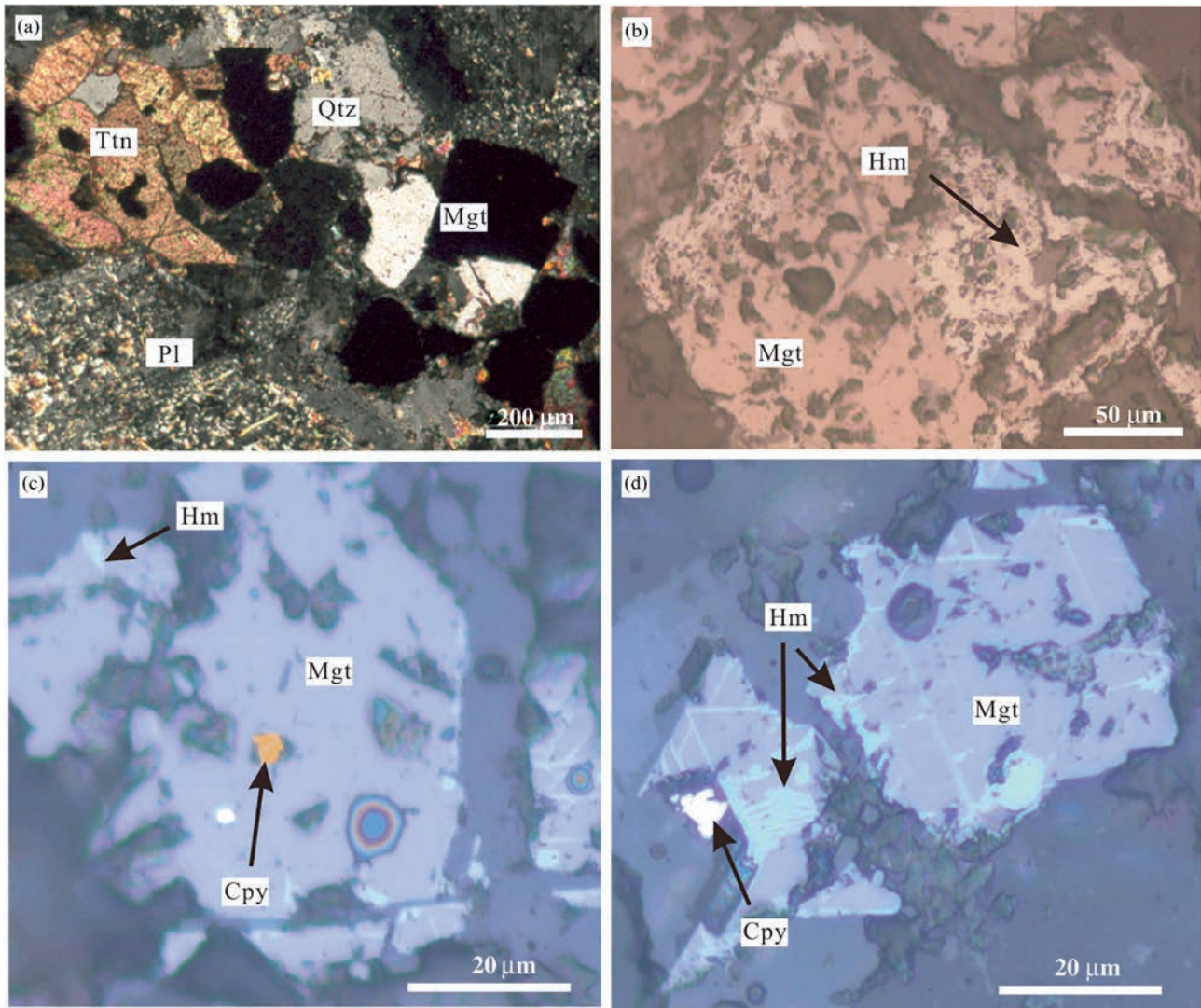
Fig. 6. Photos showing mineral assemblage of hornblende granite and diorite porphyry. (a) Titanite–magnetite–quartz assemblage in hornblende granite, (b) magnetite – hematite intergrowth in hornblende granite, (c, d) magnetite–hematite intergrowth associated chalcopyrite in diorite porphyry. Abbreviation: Qtz – quartz; Pl – plagioclase; Ttn – titanite; Mgt – magnetite; Hm – hematite; Cpy – chalcopyrite.

elliptic (Fig. 7c-1) in shape, mainly consist of liquid and <40% vapor (Fig. 7), which exhibits typically characteristics of primary fluid inclusions. These primary fluid inclusions in early magmatic minerals suggest their parental magmas were water saturated and have exsolved volatile phases during the early stage of magma evolution. These intrusions were generated from water-rich magmas. The melts are characterized by a high water content, and the early stage exsolution of volatiles may have resulted in the enrichment of Cu and Au during evolution of the melt and subsequent formation of porphyry Cu(Au) deposits.

6.3. Age of metallogenesis

The hornblende granite and diorite porphyry underwent Cu mineralization and quartz–epidote vein alteration. It is possible that the mineralization and alteration occurred simultaneous with the Jurassic intrusions or later geological events. It is necessary to determine when mineralization and alteration occurred.

The hornblende granite and diorite porphyry are the product of high oxidized magmas. Most of the sulfur in the highly oxidized magmas occurs as sulfate, and magnetite and reduced sulfur formed as the result of sulfate redox reacting with early

crystallized ferrous-bearing minerals (i.e., $12[FeO] + SO_4^{2-} + 2H^+ = 4Fe_3O_4 + H_2S$) [42]. This reaction provided the reduced sulfur (H_2S) necessary for the formation of sulfides such as chalcopyrite. Hematite formed by the reaction of sulfate with magnetite (i.e., $38Fe_3O_4 + 6SO_4^{2-} + 5H_2O = 57Fe_2O_3 + 2S_3^- + 10OH$) [42]. These reactions may have resulted in the formation of magnetite, hematite, and chalcopyrite mineral assemblage during the later stages of magmatic evolution, and these minerals represent the early stages of mineralization in a porphyry-Cu-forming system [41,42]. The early stage Cu mineralization genetically related to high oxidized magma usually has mineral assemblage of chalcopyrite, magnetite-hematite [41,42]. Primary chalcopyrite, associated with magnetite–hematite, is present in the mineralized diorite porphyry (Fig. 6c and d), suggesting that the Cu mineralization and alteration are genetically related to the diorite porphyry.

The south Gangdese underwent mainly two stages of intrusion related Cu mineralization corresponding to subduction and collision related magmatic activities, respectively. The hornblende granite and diorite porphyry were surrounded by Cretaceous biotite–K-feldspar granite and Cenozoic biotite granites (Fig. 1c and d). Field observations indicate that only the Jurassic volcanic rocks and intrusions underwent Cu mineralization and
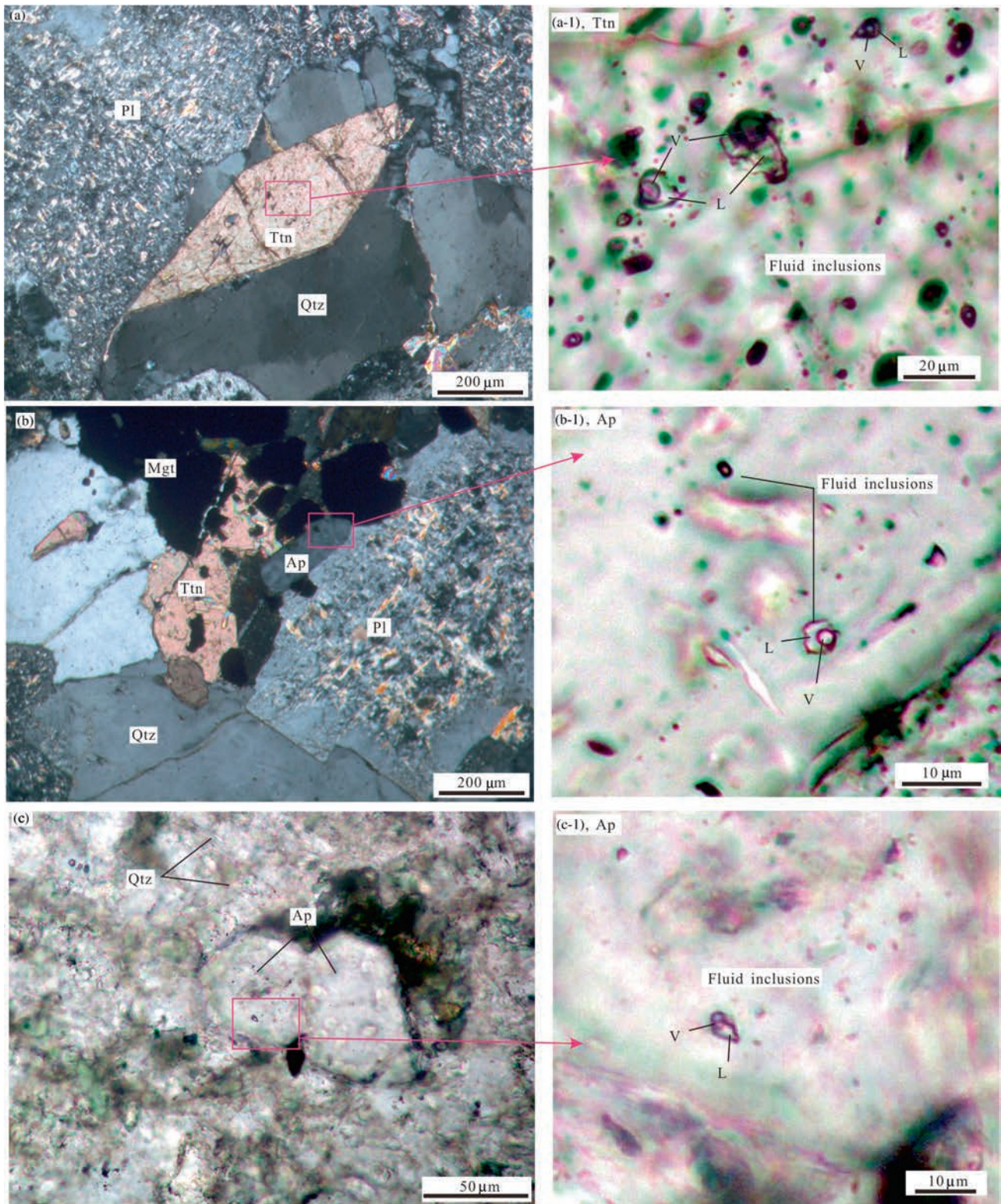
Fig. 7. Photos showing fluid inclusions in magmatic minerals. (a, a-1) Magmatic titanite of hornblende granite and fluid inclusions therein, (b, b-1) magmatic apatite of hornblende granite and fluid inclusions therein, (c, c-1) magmatic apatite of diorite porphyry and fluid inclusions therein. Abbreviation: Qtz –quartz; Pl – plagioclase; Ttn – titanite; Mgt – magnetite; Ap – apatite; V – vapor phase; L – liquid phase.

quartz–epidote vein alteration, not the Cretaceous–Cenozoic granitic batholith. This suggests that Cu mineralization and alteration occurred before the formation of the surrounding intrusions and are genetically related to their hosted rocks. The above two lines of evidences suggest that the Cu mineralization occurred simultaneously with the hosted intrusions.

6.4. Mineralization potential of subduction-related porphyry deposits in the south Gangdese

Porphyry deposits related to subduction of the Neo-Tethys oceanic crust are much smaller in size and fewer in number than those related to continental collision in the south Gangdese. Until recently, only the Xiongcun super-large porphyry Cu–Au deposit has been identified as related to Middle–Jurassic Neo-Tethys subduction in the south Gangdese [14]. To determine whether the south Gangdese is likely to host subduction-related porphyry Cu (Au) deposits, the distribution and geochemical signatures favoring porphyry mineralization should be studied in detail.

Numerous Jurassic volcanic rocks and intrusions have been reported in the south Gangdese [16,26,48–55]. Our work has identified a series of Jurassic volcanic rocks and intrusions in an area stretching from Xietongmen to Quxu (∼200 km in length; Fig. 1). The present results, combined with the findings of previous work, indicate that Early–Middle Jurassic igneous rocks are widespread in the south Gangdese, forming a subduction-related felsic igneous belt. In addition, a large proportion of the intrusions are closely associated with, and genetically related to, Cu mineralization and epidote vein alteration. These mineralized intrusions yield similar zircon ages to those of the Xiongcun porphyry Cu–Au deposit [14], suggesting that the Early–Middle Jurassic Cu(Au) mineralization, triggered by Neo-Tethys subduction, is widely distributed (>200 km in length in an E–W direction) in the south Gangdese.

Porphyry Cu(Au) deposits are genetically related to oxidized magmas with high water contents [34,36,39–42,56–58]. This relationship occurs because the behavior of chalcophile elements (e.g., Cu and Au) in magmas is strongly controlled by the sulfur species, and highly oxidizing conditions may promote the oxidation of residual sulfide in the source magmas, thereby liberating chalcophile elements [59]. Experimental work shows that Cu has a high partition coefficient between sulfide and silicate melts (e.g., $D_{\text{Cu}}^{\text{sulfide}}/_{\text{silicate melt}}$ = 550–10,000 [60,61]). More sulfur is present as sulfate, and thus sulfides remain unsaturated during fractional crystallization in highly oxidizing magmas [62,63], favoring the enrichment of Cu in residual magma and resulting in porphyry Cu mineralization. Moreover, chalcophile elements are more likely to fractionate into aqueous fluids than into melts, with $D_{\text{Cu}}^{\text{fluid}}/_{\text{silicate melt}}$ = 316–2700 [64–66]. Magmas with a high water content are expected to exsolve volatile phases earlier than dry magmas. These magmas favor the concentration of Cu in volatile phases during fractional crystallization. Given that the source magmas of the Early–Middle Jurassic mineralized intrusions in the south Gangdese are highly oxidized and have a high water content, it is reasonable to conclude that these mineralized intrusions have great potential for hosting subduction-related porphyry Cu(Au) deposits.

Typical porphyry Cu(Mo) deposits related to collisional magmatic rocks in the Gangdese belt are characterized by high positive $\varepsilon_{\text{Hf}}(t)$ and $\varepsilon_{\text{Nd}}(t)$ values [67], and there is a positive correlation between deposit size and values of $\varepsilon_{\text{Hf}}(t)$ or $\varepsilon_{\text{Nd}}(t)$. These features suggest that the magma source plays an important role in the formation of porphyry Cu deposits. The Early–Middle Jurassic intrusions in the south Gangdese typically have very high positive $\varepsilon_{\text{Hf}}(t)$ (average: +13.3) and $\varepsilon_{\text{Nd}}(t)$ (Xiongcun: +4.6–5.9) values [15,48–52], suggesting that the Early–Middle Jurassic igneous felsic intrusions originated in a region of mantle that provided metals for porphyry Cu mineralization [68,69].

Early–Middle Jurassic felsic igneous rocks that formed as a result of subduction of Neo-Tethys oceanic crust are widely distributed in the south Gangdese, and most of the intrusions host Cu mineralization. The source magmas of the Cu-mineralized intrusions were highly oxidized, had a high water content, and were derived from juvenile crust. The geochemical features and sources of the Early–Middle Jurassic felsic intrusions in the south Gangdese provide excellent conditions for the formation of porphyry Cu(Au) deposits in the south Gangdese.

6.5. Geological implications

All the available evidence indicates that the Jurassic magmatic activities in the southern Gangdese region has good potential for subduction-related porphyry Cu(Au) deposits. Many Early–Middle Jurassic felsic igneous rocks were reported in the south Gangdese, but why only the Xiongcun intrusions produced a giant porphyry Cu(Au) deposit and where is the favorable target domains for subduction related porphyry Cu(Au) deposits?

It is well known that porphyry copper deposits were emplaced at a depth of 1–3 km. Plutons, like granites and diorites, were emplaced much deeper than porphyries. Widespread Cenozoic granite batholiths in the south Gangdese region suggest that the area underwent large-scale uplift and denudation after the Cenozoic [9,70,71], resulting in erosion of much of the Early–Middle Jurassic magmatic rocks. Most of the Early-Middle Jurassic intrusions exposed in the south Gangdese are granite, tonalite, quartz monzonite and diorite [26,48–50,52,55], suggesting that most of the subduction related Jurassic porphyry Cu(Au) deposits might have been denudated. Only the porphyry deposits occurred in the depression area could be survived after large scale denudation.

The Xiongcun porphyry Cu(Au) deposit provides strong evidence that Early–Middle Jurassic porphyry Cu(Au) deposits occurred in the depression area remained across the south Gangdese region after the large-scale denudation. The association of Early–Middle Jurassic volcanic rocks and intrusions in the south Gangdese indicates that basin subsidence may have inhibited the denudation of Early–Middle Jurassic porphyry Cu(Au) ore-forming systems. Therefore, areas in the south Gangdese covered by Early–Middle Jurassic volcanic rocks, especially associated with epidote alteration and/or Cu mineralization, are the main prospecting target for subduction-related porphyry Cu(Au) deposits.

7. Conclusions

(1) A mineralized hornblende granite and a diorite porphyry were emplaced at 177.3 Ma and 166.3 Ma, respectively.
(2) The south Gangdese underwent strong Early–Middle Jurassic magmatism, and the related magmas were characterized by high oxygen fugacity and high water content, favoring the formation of porphyry Cu(Au) deposits.
(3) The majority of Early–Middle Jurassic felsic igneous rocks in the south Gangdese underwent synchronous Cu mineralization. The region has great potential for subduction-related porphyry Cu(Au) ore exploration, and the key prospecting targets should be areas covered by Jurassic volcanic rocks.

Conflict of interest

The authors declare that they have no conflict of interest.

Acknowledgments

Appendix A. Supplementary data

Supplementary data associated with this article can be found, in the online version, at http://dx.doi.org/10.1016/j.scib.2017.05.026.

References

[1] Yin A, Harrison TM. Geologic evolution of the Himalayan-Tibetan orogen. Annu Rev Earth Planet Sci 2000;28:211–80.

[2] Hou ZQ, Yang ZM, Qu XM, et al. The Miocene Gangdese porphyry copper belt generated during post-collisional extension in the Tibetan Orogen. Ore Geol Rev 2009;36:25–51.

[3] Huang WT, Liang HY, Wu J, et al. Study on the metallogenesis during the early stage of continental collision in southern Gangdese, Tibet (in Chinese). Acta Petrol Sin 2013:1439–49.

[4] Yang ZM, Hou ZQ, White NC, et al. Geology of the post-collisional porphyry copper–molybdenum deposit at Qulong, Tibet. Ore Geol Rev 2009;36:133–59.

[5] Li GM, Rui ZY. Diagenetic and mineralization ages for the porphyry copper deposits in the Gangdese matallogenic belt, southern Xizang (in Chinese). Geotecton Metal 2004;28:165–70.

[6] Lin W, Liang HY, Zhang YQ, et al. Petrochemistry and SHRIMP U-Pb zircon age of the Chongjiang ore-bearing porphyry in the Gangdese porphyry copper belt (in Chinese). Geochemic 2004;33:585–92.

[7] Meng XJ, Hou ZQ, Gao YF, et al. Re-Os dating for molybdenite from Qulong porphyry copper deposit in Gangdese metallogenic belt, Xizang and its metallogenic significance (in Chinese). Geol Rev 2003;49:660–6.

[8] Mo JH, Liang HY, Yu HX, et al. Zircon U-Pb age of biotite hornblende monzonitic granite for Chongmuda Cu-Au(Mo) deposit in Gangdese belt, Xizang, China and its implications (in Chinese). Geochem 2008;37:206–12.

[9] Rui ZY, Hou ZQ, Qu XM, et al. Metallogenetic epoch of gangdese porphyry copper belt and uplift of Qinghai-Tibet Plateau (in Chinese). Mineral Deposit 2003;22:217–25.

[10] Qu XM, Hou ZQ, Li YG. Melt components derived from a subducted slab in late orogenic ore-bearing porphyries in the Gangdese copper belt, southern Tibetan plateau. Lithos 2004;74:131–48.

[11] Xu WC, Zhang HF, Guo L, et al. Miocene high Sr/Y magmatism, south Tibet: product of partial melting of subducted Indian continental crust and its tectonic implication. Lithos 2010;114:293–306.

[12] Wang R, Richards JP, Zhou LM, et al. The role of Indian and Tibetan lithosphere in spatial distribution of Cenozoic magmatism and porphyry Cu-Mo deposits in the Gangdese belt, southern Tibet. Earth Sci Rev 2015;150:68–94.

[13] Gao YF, Hou ZQ, Kamber BS, et al. Adakite-like porphyries from the southern Tibetan continental collision zones: evidence for slab melt metasomatism. Contrib Mineral Petrol 2007;153:105–20.

[14] Tafti R, Mortensen JK, Lang JR, et al. Jurassic U-Pb and Re-Os ages for the newly discovered Xietongmen Cu-Au porphyry district, Tibet, PRC: implications for metallogenic epochs in the southern Gangdese belt. Econ Geol 2009;104:127–36.

[15] Tang JX, Lang XH, Xie FW, et al. Geological characteristics and genesis of the Jurassic No. I porphyry Cu-Au deposit in the Xiongcun district, Gangdese porphyry copper belt, Tibet. Ore Geol Rev 2015;70:438–56.

[16] Kang ZQ, Xu JF, Wilde SA, et al. Geochronology and geochemistry of the Sangri Group Volcanic Rocks, Southern Lhasa Terrane: implications for the early subduction history of the Neo-Tethys and Gangdese Magmatic Arc. Lithos 2014;200:157–68.

[17] Richards JP. Tectono-magmatic precursors for porphyry Cu-(Mo-Au) deposit formation. Econ Geol Bull Soc 2003;98:1515–33.

[18] Pan GT, Mo XX, Hou ZQ, et al. Spatial-temporal framework of the Gangdese orogenic belt and itsevokution (in Chinese). Acta Petrol Sin 2006;22:521–33.

[19] Liu CZ, Chung SL, Wu FY, et al. Tethyan suturing in Southeast Asia: zircon U-Pb and Hf-O isotopic constraints from Myanmar ophiolites. Geology 2016;44:311–4.

[20] Mo XX, Dong GC, Zhao ZD, et al. Spatial and temporal distribution and characteristics of granitoids in the Gangdese Tibet and implication for crustal growth and evolution. Geol J Chin Univ 2005;11:281–90.

[21] Zhao ZD, Mo XX, Dilek Y. Geochemical and Sr-Nd-Pb-O isotopic compositions of the post-collisional ultrapotassic magmatism in SW Tibet: petrogenesis and implications for India intra-continental subduction beneath southern Tibet. Lithos 2009;113(1–2):190–212.

[22] Mo XX, Dong GC, Zhao ZD, et al. Timing of magma mixing in the gangdisê magmatic belt during the India-Asia collision: zircon SHRIMP U-Pb dating (in chinese). Acta Geol Sin 2005;79:66–76.

[23] Zhu DC, Pan GT, Chung SL, et al. SHRIMP zircon age and geochemical constraints on the origin of lower Jurassic volcanic rocks from the Yeba formation, Southern Gangdese, south Tibet. Int Geol Rev 2008;50:442–71.

[24] Ji WQ, Wu FY, Chung SL, et al. The Gangdese magmatic constraints on a latest Cretaceous lithospheric delamination of the Lhasa terrane, southern Tibet. Lithos 2014;210:168–80.

[25] Ma L, Wang Q, Wyman DA, et al. Late Cretaceous (100–89Ma) magnesian charnockites with adakitic affinities in the Milin area, eastern Gangdese: partial melting of subducted oceanic crust and implications for crustal growth in southern Tibet. Lithos 2013;175–176:315–32.

[26] Wen DR, Liu DY, Chung SL, et al. Zircon SHRIMP U-Pb ages of the Gangdese Batholith and implications for Neo-tethyan subduction in southern Tibet. Chem Geol 2008;252:191–201.

[27] Chiu HY, Chung SL, Wu FY, et al. Zircon U-Pb and Hf isotopic constraints from eastern Transhimalayan batholiths on the pre-collisional magmatic and tectonic evolution in southern Tibet. Tectonophysics 2009;477:3–19.

[28] Tang JX, Li FJ, Li ZJ, et al. Time limit for formation of main geological bodies in Xiongcun copper-gold deposit, Xietongmen County, Tibet: evidence from zircon U-Pb ages and Re-Os age of molybdenite (in Chinese). Miner Deposit 2010:461–75.

[29] Zou YQ, Huang WT, Liang HY, et al. Identification of porphyry fenetically associated with mineralization and its zircon U-Pb and biotite Ar-Ar age of the Xiongcun Cu-Au deposit, southern Gangdese, Tibet (in Chinese). Acta Petrol Sin 2015:2053–62.

[30] Tang JX, Huang Y, Li ZJ, et al. Element geochemical characteristics of Xiongcun Cu-Au deposit in Xaitongmoin County, Tibet (in Chinese). Miner Deposit 2009;28:15–28.

[31] Zhao Y, Sun Y, Yan JH, et al. The Archean-Paleoproterozoic crustal evolution in the Dunhuang region, NW China: constraints from zircon U-Pb geochronology and in situ Hf isotopes. Precambrian Res 2015;271:83–97.

[32] Liu YS, Hu ZC, Zong KQ, et al. Reappraisement and refinement of zircon U-Pb isotope and trace element analyses by LA-ICP-MS. Chin Sci Bull 2010;55:1535–46.

[33] Ludwig K. ISOPLOT 3.0: A Geochronological Toolkit for Microsoft Excel. Berkeley, California: Berkeley Geochronology Center; 2003.

[34] Liang HY, Campbell IH, Allen C, et al. Zircon Ce^{4+}/Ce^{3+} ratios and ages for Yulong ore-bearing porphyries in eastern Tibet. Miner Deposit 2006;41:152–9.

[35] Harris AC, Allen CM, Bryan SE, et al. ELA-ICP-MS U-Pb zircon geochronology of regional volcanism hosting the Bajo de la Alumbrera Cu-Au deposit: implications for porphyry-related mineralization. Miner Deposit 2004;39:46–67.

[36] Ballard JR, Palin MJ, Campbell IH. Relative oxidation states of magmas inferred from Ce(IV)/Ce(III) in zircon: application to porphyry copper deposits of northern Chile. Contrib Mineral Petrol 2002;144:347–64.

[37] Cline JS. Geology. How to concentrate copper. Science 2003;302:2075–6.

[38] Kelley KA, Cottrell E. Water and the oxidation state of subduction zone magmas. Science 2009;325:605–7.

[39] Sillitoe RH. Porphyry copper systems. Econ Geol 2010;105:3–41.

[40] Sun WD, Huang RF, Li H, et al. Porphyry deposits and oxidized magmas. Ore Geol Rev 2015;65:97–131.

[41] Liang HY, Sun WD, Su WC, et al. Porphyry copper-gold mineralization at Yulong, China, promoted by decreasing redox potential during magnetite alteration. Econ Geol 2009;104:587–96.

[42] Sun WD, Liang HY, Ling MX, et al. The link between reduced porphyry copper deposits and oxidized magmas. Geochim Cosmochim Acta 2013;103: 263–75.

[43] Trail D, Bruce WE, Tailby ND. Ce and Eu anomalies in zircon as proxies for the oxidation state of magmas. Geochim Cosmochim Acta 2012;97:70–87.

[44] Harlov D, Tropper P, Seifert W, et al. Formation of Al-rich titanite ($CaTiSiO_4O – CaAlSiO_4OH$) reaction rims on ilmenite in metamorphic rocks as a function of fH_2O and fO_2. Lithos 2006;88:72–84.

[45] Piccoli P, Candela P, Rivers M. Interpreting magmatic processes from accessory phases: titanite a small-scale recorder of large-scale processes. T Roy Soc Edin Earth 2000;91:257–67.

[46] Wones DR. Significance of the assemblage titanite + magnetite + quartz in granitic rocks. Am Mineral 1989;74:744–9.

[47] Wu J, Liang HY, Huang WT, et al. Identification of coesite-bearing amphibolite in the North Qinling and its geological significance (in Chinese). Chin Sci Bull 2012;57:1126–36.

[48] Chu MF, Chung SL, Song BA, et al. Zircon U-Pb and Hf isotope constraints on the Mesozoic tectonics and crustal evolution of southern Tibet. Geology 2006;34:745–8.

[49] Guo LS, Liu YL, Liu SW, et al. Petrogenesis of Early to Middle Jurassic granitoid rocks from the Gangdese belt, Southern Tibet: implications for early history of the Neo-Tethys. Lithos 2013;179:320–33.

[50] Ji WQ, Wu FY, Chung SL, et al. Zircon U-Pb geochronology and Hf isotopic constraints on petrogenesis of the Gangdese batholith, southern Tibet. Chem Geol 2009;262:229–45.

[51] Zhang HF, Xu WC, Guo JQ, et al. Zircon U-Pb isotopic composition of deformed granite in the southern margin of the Gangdese belt, Tibet: evidence for early Jurassic subduction of Neo-Tethyan oceanic slab (in Chinese). Acta Petrol Sin 2007;23:1347–53.

[52] Meng YK, Dong HW, Cong Y, et al. The early-stage evolution of the Neo-Tethys ocean: evidence from granitoids in the middle Gangdese batholith, southern Tibet. J Geodyn 2016;94–95:34–49.

[53] Meng YK, Xu ZQ, Santosh M, et al. Late Triassic crustal growth in southern Tibet: evidence from the Gangdese magmatic belt. Gondwana Res 2015;37:449–64.

[54] Dong YH, Xu JF, Zeng QG, et al. Is there a Neo-Tethys' subduction record earlier than arc volcanic rocks in the Sangri Group (in chinese)? Acta Petrol Sin 2006;22:661–8.

[55] Hu JX, Chen JL, Zhang ZW, et al. Geochemistry and genesis of Middle Jurassic adakitic rocks in the Xietongmen area of southern Tibet (in Chinese). Geotecton Metal 2013;37:320–32.

[56] Mungall JE. Roasting the mantle: slab melting and the genesis of major Au and Au-rich Cu deposits. Geology 2002;30:915–8.

[57] Huang WT, Wu J, Zhang J, et al. Geochemistry and Hf–Nd isotope characteristics and forming processes of the Yuntoujie granites associated with W-Mo deposit, Guangxi, South China. Ore Geol Rev 2016;81 (part2):953–64.

[58] Liang HY, Mo JH, Hu GQ. New mechanism of ore forming elements precipitation in porphyry copper (gold) deposit and its prospecting significance (in Chinese). Miner Deposit 2010:233–4.

[59] Sillitoe RH. Characteristics and controls of the largest porphyry copper–gold and epithermal gold deposits in the circum–Pacific region. Aust J Earth Sci 1997;44:373–88.

[60] Gaetani GA, Grove TL. Partitioning of moderately siderophile elements among olivine, silicate melt, and sulfide melt: constraints on core formation in the Earth and Mars. Geochim Cosmochim Acta 1997;61:1829–46.

[61] Jugo PJ, Candela PA, Piccoli PM. Magmatic sulfides and Au: Cu ratios in porphyry deposits: an experimental study of copper and gold partitioning at 850°C, 100 MPa in a haplogranitic melt–pyrrhotite–intermediate solid solution–gold metal assemblage, at gas saturation. Lithos 1999;46:573–89.

[62] Mungall JE, Hanley JJ, Arndt NT, et al. Evidence from meimechites and other low-degree mantle melts for redox controls on mantle-crust fractionation of platinum-group elements. Proc Natl Acad Sci USA. 2006;103:12695–700.

[63] Sun WD, Arculus RJ, Kamenetsky VS, et al. Release of gold-bearing fluids in convergent margin magmas prompted by magnetite crystallization. Nature 2004;431:975–8.

[64] Keppler H, Wyllie PJ. Partitioning of Cu, Sn, Mo, W, U, and Th between melt and aqueous fluid in the systems haplogranite-H_2O-HCl and haplogranite-H_2O-HF. Contrib Mineral Petrol 1991;109:139–50.

[65] Simon AC, Pettke T, Candela PA, et al. Copper partitioning in a melt-vapor-brine-magnetite-pyrrhotite assemblage. Geochim Cosmochim Acta 2006;70:5583–600.

[66] Zajacz Z, Halter WE, Pettke T, et al. Determination of fluid/melt partition coefficients by LA-ICPMS analysis of co-existing fluid and silicate melt inclusions: controls on element partitioning. Geochim Cosmochim Acta 2008;72:2169–97.

[67] Hou ZQ, Yang ZM. Porphyry deposits in continental settings of China: geological characteristics, magmatic-hydrothermal system, and metallogenic model (in Chinese). Acta Geol Sin 2009;83:1779–817.

[68] Lee CTA, Anderson DL. Continental crust formation at arcs, the arclogite "delamination" cycle, and one origin for fertile melting anomalies in the mantle. Sci Bull 2015;60:1141–56.

[69] Niu YN. Testing the geologically testable hypothesis on subduction initiation. Sci Bull 2016;61:1231–5.

[70] Zhang XM, Sun RM, Teng JW. Study on crustal, lithospheric and asthenospheric thickness beneath the Qinghai-Tibet Plateau and its adjacent areas. Chin Sci Bull 2007;52:797–804.

[71] Zheng Y, Zhang JJ, Wang JM, et al. Rapid denudation of the Himalayan orogen in the Nyalam area, southern Tibet, since the Pliocene and implications for tectonics–climate coupling. Chin Sci Bull 2014;59:874–85.